Physics of the Earth and Planetary Interiors 255 (2016) 50–65

Contents lists available at ScienceDirect

Physics of the Earth and Planetary Interiors

journal homepage: www.elsevier.com/locate/pepi

The observational signature of modelled torsional waves and comparison to geomagnetic jerks

G.A. Cox *, P.W. Livermore, J.E. Mound

School of Earth and Environment, University of Leeds, Leeds LS2 9JT, UK

ARTICLE INFO

Article history:
Received 26 January 2016
Received in revised form 23 March 2016
Accepted 25 March 2016
Available online 9 April 2016

Keywords:
Geomagnetism
Geomagnetic jerks
Torsional waves
Secular variation

ABSTRACT

Torsional Alfvén waves involve the interaction of zonal fluid flow and the ambient magnetic field in the core. Consequently, they perturb the background magnetic field and induce a secondary magnetic field. Using a steady background magnetic field from observationally constrained field models and azimuthal velocities from torsional wave forward models, we solve an induction equation for the wave-induced secular variation (SV). We construct time series and maps of wave-induced SV and investigate how previously identified propagation characteristics manifest in the magnetic signals, and whether our modelled travelling torsional waves are capable of producing signals that resemble jerks in terms of amplitude and timescale. Fast torsional waves with amplitudes and timescales consistent with a recent study of the 6 yr ΔLOD signal induce very rapid, small (maximum ∼2 nT/yr at Earth's surface) SV signals that would likely be difficult to be resolve in observations of Earth's SV. Slow torsional waves with amplitudes and timescales consistent with other studies produce larger SV signals that reach amplitudes of ∼20 nT/yr at Earth's surface. We applied a two-part linear regression jerk detection method to the SV induced by slow torsional waves, using the same parameters as used on real SV, which identified several synthetic jerk events. As the local magnetic field morphology dictates which regions are sensitive to zonal core flow, and not all regions are sensitive at the same time, the modelled waves generally produce synthetic jerks that are observed on regional scales and occur in a single SV component. However, high wave amplitudes during reflection from the stress-free CMB induce large-scale SV signals in all components, which results in a global contemporaneous jerk event such as that observed in 1969. In general, the identified events are periodic due to waves passing beneath locations at fixed intervals and the SV signals are smoothly varying. These smooth signals are more consistent with the geomagnetic jerks envisaged by Demetrescu and Dobrica than the sharp 'V' shapes that are typically associated with geomagnetic jerks.

1. Introduction

Satellite and ground-based observations show that temporal fluctuations in the geomagnetic field occur on a wide range of time scales, from daily interactions with the ionosphere to the millions of years between polarity reversals. Most changes at approximately annual to centennial timescales, called secular variation (SV), is associated with the geodynamo, the process that generates a large-scale self-sustaining magnetic field from fluid motion inside Earth's outer core (Larmor, 1919; Elsasser, 1946). However, progress in understanding the dynamics of Earth's core, and the associated signals in the geomagnetic field, is hindered by the fact that the core is too remote to be probed directly and that numerical dynamo simulations are unable to reach the relevant parameter regime due to computational limitations (Davies et al., 2011; King and Buffett, 2013). The most rapid observed feature of the core-generated magnetic field are geomagnetic jerks. These are abrupt jumps in the second time-derivative (secular acceleration, SA) of Earth's magnetic field, which correspond to sharp changes in the trend of the first time-derivative of the magnetic field (SV) (Courtillot et al., 1978; Mandea et al., 2010). Jerks separate periods of almost steady SA so that the SV appears as a series of straight-line segments separated by the jerk itself, see Fig. 1 for several examples of jerks in the East (Y) component of SV at four European observatories. Several jerks are known to have occurred in the twentieth and twenty first centuries, including those in 1969 (Courtillot et al., 1978; Malin et al., 1983; Whaler, 1987), 1978 (Gubbins and Tomlinson, 1986; Davis and Whaler, 1997), 1991 (Macmillan, 1996), 1999 (Mandea et al., 2000) and 2003 (Olsen

* Corresponding author at: School of Environmental Sciences, University of Liverpool, Liverpool L69 3GP, UK.

http://dx.doi.org/10.1016/j.pepi.2016.03.012
0031-9201/

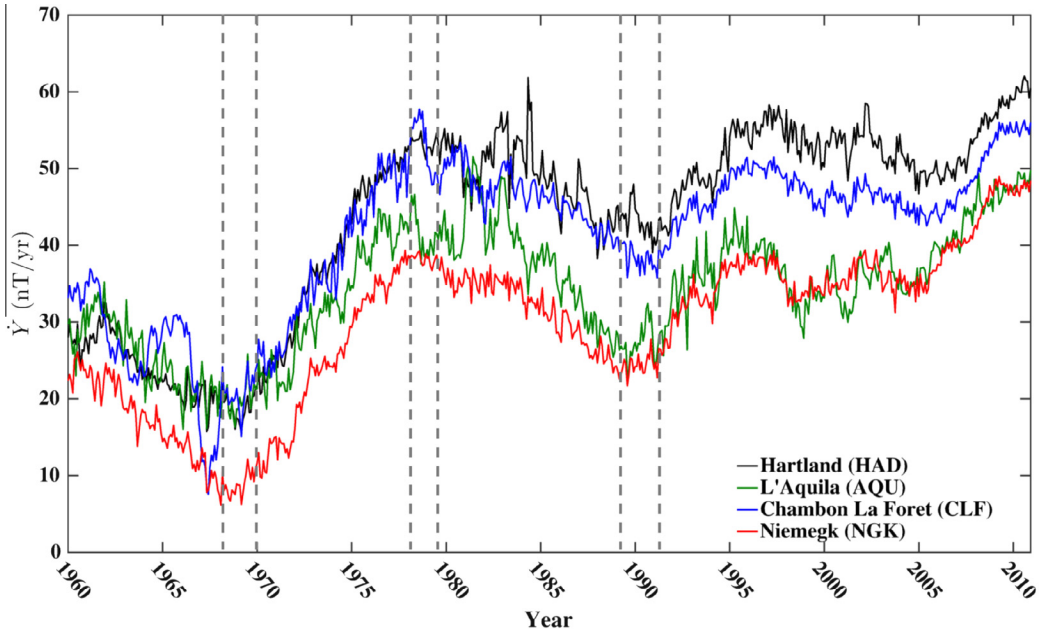

Fig. 1. The Y component of SV, calculated as annual differences of monthly means, at four different observatories in Europe. The black line is Hartland (HAD), the green line is L'Aquila (AQU), the blue line is Chambon La Forêt (CLF) and the red line is Niemegk (NGK). The vertical dashed lines (grey) indicate approximate timings of three observed geomagnetic jerks. (For interpretation of the references to color in this figure legend, the reader is referred to the web version of this article.)

and Mandea, 2007). According to Alexandrescu et al. (1996), who used wavelet analysis to detect and characterise worldwide jerk occurrences, some are observed globally and others only regionally.

Despite many attempts, the physical origin of geomagnetic jerks is yet to be established, see Mandea et al. (2010) for a thorough review of this topic. Malin and Hodder (1982) used spherical harmonic analysis to establish that jerks are of internal origin, but none of the subsequently proposed generating mechanisms has proved completely successful. The previous interpretations of jerks include core flows (e.g., Le Huy et al. (1998), Wardinski et al. (2008), and Silva and Hulot (2012)), torsional oscillations (Bloxham et al., 2002) and instability of an Ekman–Hartman boundary layer at the CMB (Desjardins et al., 2001). Of particular interest to this work are those interpretations that rely upon zonal core flows and/or torsional Alfvén waves, a type of magnetohydrodynamic wave that is predicted to exist in Earth's core on decadal timescales (Braginsky, 1970, 1984), identified in dynamo models (Wicht and Christensen, 2010; Teed et al., 2013, 2015), and inferred from various geophysical datasets (e.g., Hide et al., 2000; Zatman and Bloxham, 1997, 1999; Buffett et al., 2009; Gillet et al., 2010).

Several authors (Waddington et al., 1995; Bloxham et al., 2002; Olsen and Mandea, 2008) have shown that no steady flow can produce jerk-like features, nor can a steady flow in a drifting frame (Holme and Whaler, 2001). This implies that a steady flow of the magnitude typically assumed for core flow, $\mathcal{O}(10^{-4})$ m/s, is not able to produce the strong SA associated with jerks and that flow acceleration is likely an important contribution to jerks (Waddington et al., 1995). Bloxham et al. (2002) relaxed the steady flow constraint and showed that some jerks can be explained by the combination of a steady flow and a simple time-varying, axisymmetric, equatorially symmetric, toroidal zonal flow. Such flows are consistent with torsional oscillations (torsional wave normal modes) and give an excellent fit to many jerk features, particularly in Europe, though the predicted SV was notably smoother than the observations. The authors also noted that the SV generated by simple core flows depends on the local morphology of the ambient magnetic field. This is a crucial point because it means that large-scale core flow can produce localised signals at magnetic observatories and thus there is no need to invoke a small-scale core flow to explain those jerk events that are observed on a regional scale. However, whilst the simple zonal flows consistent with torsional waves are likely an important contribution, a radial component to flow is required to explain jerks (Lesur et al., 2015). Less restrictive flows, such as toroidal or tangentially geostrophic flows, are needed to reproduce all of the observed features of SV (e.g., Wardinski et al., 2008; Silva and Hulot, 2012). Toroidal flows have no radial (poloidal) component and are consistent with a stratified layer at the top of the outer core, which was proposed by, among others, Whaler (1980) and Braginsky (1999). More recently, various authors (e.g., Helffrich and Kaneshima (2013), Gubbins and Davies (2013), and Buffett (2014)) have advocated a stratified layer in the outer core using seismological evidence, geomagnetic observations, and material properties of liquid iron at high temperature and pressure. Tangentially geostrophic flows neglect the Lorentz term in the force balance at the top of the core, implying a zeroth order balance between the horizontal components of the pressure gradient and the Coriolis force (Le Mouël, 1984). This flow is also consistent with a stratified layer beneath the CMB (Jault and Le Mouël, 1991), though this constraint is less restrictive than the purely toroidal case because it allows a poloidal component. An intermediary flow that is more general than pure torsional oscillations but more restrictive than tangential geostrophy is also able to explain observed SV, including geomagnetic jerks. These are called quasi-geostrophic flows (Gillet et al., 2009) and are almost invariant along the rotation axis. See Holme (2015) for a recent review of fluid motions in the outer core and previous core flow modelling attempts.

The aim of this paper is to use the forward models of Cox et al. (2014, hereafter CLM) to establish the nature of torsional wave-induced SV at the core–mantle-boundary and at the Earth's surface. Of particular interest to this work are the effects of the background magnetic field morphology on sensitivity to zonal core flows, and the influence of wave propagation speeds and amplitude scalings on the characteristics of the modelled SV. The wave propagation velocity is determined by the strength of the ambient mag-

netic field inside the core, a value that was recently revised upwards on the basis of torsional waves inferred from observations (Gillet et al., 2010) and remains the subject of some debate. The modelled wave amplitudes must be scaled because the torsional wave equation has no intrinsic scale. Based on previously observationally-constrained studies of torsional waves (or torsional normal modes), we consider two different scalings for our modelled waves: first, 'fast', low amplitude waves and second, 'slow', high amplitude waves. The 'fast' waves were scaled for consistency with recent studies on torsional waves by Gillet et al. (2010) and Gillet et al. (2015), having a 6 yr core transit time, implying a strong internal magnetic field, and a relatively low maximum amplitude of approximately ±0.4 km/yr. The 'slow' waves were chosen for consistency with various other studies, having a 60 yr core transit time and maximum amplitudes of approximately ±4 km/yr. The first study of torsional oscillations in Earth's core by Braginsky (1970) theoretically predicted torsional oscillations with a period of approximately 60 years. The same period was recently advocated by Roberts et al. (2007), based on empirical mode decomposition of ΔLOD and SV data. Zatman and Bloxham (1997) identified two torsional modes with periods of 76 and 53 years, respectively, based on observational data, giving an average period of 60–65 years. A subsequent study by Hide et al. (2000) identified a robust 65 year torsional oscillation period using core angular momentum estimates obtained as follows: the observationally-constrained geomagnetic field model of Jackson et al. (1993), *gufm1*, was used to reconstruct the SV at the core–mantle-boundary, which was then inverted for the flow at the top of the core. Assuming the axisymmetric zonal flows were associated with torsional waves, the flow field inside the core was also inferred, and the angular momentum of the flow field was calculated and compared to observations of LOD. The theoretical study of Mound and Buffett (2005) used Green's functions to show how torsional oscillations might be excited in the core, and a subsequent study by the same authors identified several periods associated with torsional oscillations (Mound and Buffett, 2007). Their first four modes had approximate periods of 80, 46, 32 and 24 years respectively. Dickey and de Viron (2009) reviewed the leading modes of torsional oscillations found in previous studies, from both observational and theoretical methods, and also isolated some additional modes using the core angular momentum estimates of Hide et al. (2000). Their first two modes were in agreement with the previous results of Zatman and Bloxham (1997) and Mound and Buffett, 2007. Note that Buffett (2014) has attributed the 60 yr core signal to another type of waves, called Magneto-Archimedes–Coriolis (MAC) waves, that may propagate in a stably stratified layer at the top of the outer core. However, there is a substantial body of work linking the 60 yr signal with torsional waves and for the purposes of this study, that is what we will assume here. Having produced synthetic SV signals for both 'fast' and 'slow' torsional waves, we apply the jerk detection method developed by Brown et al. (2013) and examine the proposed link between torsional waves and jerks.

The remainder of this paper is structured as follows: Section 2 provides a brief overview of the torsional wave forward models (the reader is referred to CLM for a detailed discussion of this subject); the method used to calculate wave-induced SV and the resulting synthetic signals are presented in Section 3; the paper closes with 'discussion and conclusions' in Section 4.

2. Method

In CLM, we presented the results of 1-D forward models of travelling torsional waves and discussed their propagation in Earth's core. These models were produced by solving the canonical torsional wave equation, which is defined in cylindrical coordinates $(s,\ \phi,\ z)$ as

$$\frac{\partial^2 u_\phi}{\partial t^2} = \frac{1}{s^2 \mu_0 \rho_0 z_T} \frac{\partial}{\partial s}\left(s^3 z_T \{B_s^2\} \frac{\partial \left(\frac{u_\phi}{s}\right)}{\partial s} \right), \tag{1}$$

where u_ϕ is the azimuthal velocity, μ_0 is the permeability of free space, ρ_0 is the reference density (taken as 9900 kg/m^3), z_T is the half height of the geostrophic cylinder (a function of s in a spherical core) and $\{B_s^2\}$ is the square of the s-component of the magnetic field averaged over a geostrophic cylinder surface (Braginsky, 1970; Jault and Légaut, 2005; Roberts and Aurnou, 2011). The equation was solved using a third-order Adams–Bashforth finite difference scheme on a staggered grid and the time evolution started from a Gaussian-like profile given by

$$u_\phi = As^2(s-c)^2 e^{-\left(\frac{s-(c/2)}{\sigma}\right)^2}, \tag{2}$$

where c is the radius of the outer core (3480 km), A is the amplitude, chosen for consistency with various previous works (e.g., Braginsky, 1970; Zatman and Bloxham, 1997, 1999; Hide et al., 2000; Roberts et al., 2007; Dickey and de Viron, 2009; Gillet et al., 2010), and σ determines the width of the pulse. This initial profile is a smooth bell-shaped curve that is centred about $c/2$, the midpoint of the core. A stress-free condition was imposed at the equator of the core–mantle-boundary (CMB), following Canet et al. (2009), and the regularity condition $u_\phi = 0$ is obeyed at Earth's rotation axis (see Lewis and Bellan (1990) and CLM for further details). The Adams–Bashforth finite difference code was benchmarked against known analytic solutions for torsional waves in a cylinder (constant z_T, Mound and Buffett (2007)). Note that the above equation is valid for an incompressible fluid and does not include viscosity or dissipation terms that take into account coupling between the core and the mantle or between the inner core and the outer core.

Under the frozen-flux approximation, fluid in the outer core is assumed to be perfectly conducting and magnetic field lines are tied into the fluid. Since the mantle is presumed to be an electrical insulator, there is a jump in electrical conductivity across the CMB which means that only the radial component of the magnetic field is guaranteed to be continuous across this boundary (e.g., Whaler and Holme, 2007). Here we assume that fluid motions interact with the radial magnetic field through the radial component of the diffusionless version of the induction equation. The frozen-flux form of the induction equation at the CMB is

$$\frac{\partial B_r}{\partial t} = -\nabla_{\boldsymbol{H}} \cdot (\boldsymbol{u} B_r), \tag{3}$$

e.g., Roberts and Scott (1965) and Backus (1968), where $\nabla_{\boldsymbol{H}}\cdot$ is the horizontal divergence operator. For an arbitrary vector, $\boldsymbol{A}$, defined in spherical coordinates $(r,\ \theta,\ \phi)$, $\nabla_{\boldsymbol{H}} \cdot \boldsymbol{A} = \frac{1}{r\sin\theta}\frac{\partial(A_\theta \sin\theta)}{\partial\theta} + \frac{1}{r\sin\theta}\frac{\partial A_\phi}{\partial\phi}$.

The total magnetic field is the sum of the steady background field $\boldsymbol{B}$ and a small perturbation $\boldsymbol{b}$. In the following discussion, we assume that this perturbation to the magnetic field is caused by flow associated with torsional waves, u_ϕ. Therefore, the equation to be solved is a linearisation of (3) when $\boldsymbol{u}$ and $\boldsymbol{b}$ are small:

$$\frac{\partial b_r}{\partial t} = -\frac{u_\phi}{s}\frac{\partial B_r}{\partial \phi} \tag{4}$$

where the radius in cylindrical coordinates is linked to the radius in a spherical coordinate system by the relation $s = r\sin\theta$, (e.g., Canet et al., 2009).

We assume that the mantle is electrically insulating, thus the vector fields $\boldsymbol{B}$ and $\boldsymbol{b}$ are both related to scalar potential fields, V and v respectively, that can be expressed as sums of spherical harmonics and Gauss coefficients such that, for example, the radial

component of the steady background magnetic field at the CMB ($r = c$) is

$$B_r = -\frac{\partial V}{\partial r} = \sum_{l=1}^{\infty}\sum_{m=0}^{l}(l+1)\left(\frac{a}{c}\right)^{l+2}\left[G_l^m \cos m\phi + H_l^m \sin m\phi\right]P_l^m(\cos\theta), \quad (5)$$

where a is the radius of the Earth, $P_l^m(\cos\theta)$ is the associated Legendre function in $\cos\theta$ of degree l and order m and G_l^m and H_l^m are the Gauss coefficients. These are usually denoted using lower case g_l^m and h_l^m, but we use upper case letters here to avoid confusion with the expansion of b_r below, which uses a different set of Gauss coefficients denoted g_l^m and h_l^m. Using a similar expansion for the perturbation to the main field gives an expression for the temporal derivative of b_r at the CMB

$$\frac{\partial b_r}{\partial t} = \sum_{l=1}^{\infty}\sum_{m=0}^{l}(l+1)\left(\frac{a}{c}\right)^{l+2}\left[\dot{g}_l^m \cos m\phi + \dot{h}_l^m \sin m\phi\right]P_l^m(\cos\theta), \quad (6)$$

where g_l^m and h_l^m are the Gauss coefficients associated with $\boldsymbol{b}$.

Substituting Eqs. (5) and (6) into (4), multiplying by $P_{l'}^{m'}(\cos\theta)\cos m'\phi$, integrating over the CMB (a spherical surface) and using the orthogonality properties of the Schmidt quasi-normalised spherical harmonics gives

$$\frac{4\pi l'}{2l'+1}(l'+1)\left(\frac{a}{c}\right)^{l'+2}\dot{g}_{l'}^{m'} = -\int_0^{\pi}\frac{u_\phi \pi}{r\sin\theta}\left[\sum_{l\geqslant m'}^{\infty}(l+1)\left(\frac{a}{c}\right)^{l+2}H_l^{m'}P_l^{m'}(\cos\theta)\right]m' P_{l'}^{m'}(\cos\theta)\sin\theta d\theta. \quad (7)$$

This contains only one quantity, u_ϕ, that is not defined on a spherical surface, which is given as a function of cylindrical radius s in the previously presented 1-D forward wave models. These velocities $u_\phi(s)$ are mapped onto a grid in θ and ϕ by assuming that the velocity may be represented as a linear sum of zonal spherical harmonics ($m = 0$) such that

$$u_\phi(s) = \sum_{k=1}^{\infty} a_k P_k^0(\cos\theta), \quad (8)$$

where a_k is the contribution of a particular mode k. Orthogonality properties are then used to derive an expression for each coefficient a_k up to the maximum number of modes used in the projection, which is chosen to give a converged solution and is typically set at 100 modes. For each order m', we then calculate the sum in square brackets at each θ node

$$\dot{g}_{l'}^{m'} = -\frac{2l'+1}{4a(l'+1)}\left(\frac{c}{a}\right)^{l'+2} m' \int_0^{\pi}\frac{u_\phi}{r\sin\theta} \times \left[\sum_{l\geqslant m'}^{\infty}(l+1)\left(\frac{a}{c}\right)^{l+2}H_l^{m'}P_l^{m'}(\cos\theta)\right]P_{l'}^{m'}(\cos\theta)\sin\theta d\theta. \quad (9)$$

and use Gauss–Legendre quadrature to evaluate the integral and obtain the $\dot{g}_{l'}^{m'}$. A similar expression for the $\dot{h}_l^m$ coefficients is obtained by multiplying the induction equation by $P_{l'}^{m'}(\cos\theta)\sin m'\phi$ rather than $P_{l'}^{m'}(\cos\theta)\cos m'\phi$.

The background magnetic field $\boldsymbol{B}$ is specified up to spherical harmonic degree 14, which is the maximum degree to which the internally generated field is robustly determined in field models. The Gauss nodes and weights were computed using the eigenvalue method of Golub and Welsch (1969) and, in all models, sufficient nodes were used to ensure convergence of the projection of $u_\phi(s)$ onto spherical harmonics. Convergence of the velocity expansion was ensured by calculating the spatial power spectra and comparing the power contained at low and high spherical harmonic degrees at different times during wave propagation. Similarly, spatial power spectra were used to compare the magnitudes of the Gauss coefficients of the calculated wave-induced SV and determine the resolution required for the calculation of $\dot{\boldsymbol{b}}$. The power spectrum of $\dot{\boldsymbol{b}}$ was calculated at different times throughout the wave evolution in order to ensure that the resolution required for the SV induced by the initial profile is sufficient to resolve the SV induced by the waves at any time in the model. Typical convergence requires $\dot{\boldsymbol{b}}$ to calculated at 30 modes.

2.1. Background magnetic fields

The production of synthetic data relies upon zonal velocities obtained from our torsional wave forward models and upon a background magnetic field defined by Gauss coefficients (G_l^m and H_l^m in the previous section) obtained from a field model. The choice of background field will obviously influence the wave-induced SV (see Eq. (4) and Bloxham et al. (2002)), so we investigated the effects of different field models, and of using a snapshot of the observed field as opposed to a time-averaged field. As torsional waves are thought to occur on decadal timescales, and have been associated with 6 year signals in ΔLOD and SV (Gillet et al., 2010), and with geomagnetic jerks (Bloxham et al., 2002), this work only considers magnetic field models with high spatial and temporal resolution. High spatial resolution permits investigation of small-length scale features, and high temporal resolution is required because we consider the effects of using a single snapshot of the field versus a time-averaged field. Two magnetic field models were chosen as the starting point for the steady background field required for torsional wave-induced SV; CHAOS-4 by Olsen et al. (2014) and COV-OBS by Gillet et al. (2013). The CHAOS-4 model covers the period 1997–2013 and is constrained by Ørsted, CHAMP and SAC-C satellite data, augmented by monthly mean values from observatories. The COV-OBS family of models, spanning the period 1840–2010, takes a stochastic approach that uses time covariance functions to integrate some prior information on the time evolution of the geomagnetic field.

Despite the fundamental differences in model construction between the CHAOS-4 and COV-OBS models, the resulting magnetic fields look very similar when evaluated using Gauss coefficients from each model for the same time interval. Indeed, when the radial magnetic field, B_r, is constructed at the CMB for the same time, the maximum amplitude of the difference between the two fields is approximately 7% of the total field strength. This led to the conclusion that there is no reason to prefer one model over the other when looking at single snapshots of the geomagnetic field. In terms of temporal variations, the background magnetic field is considered constant over the timescales of torsional wave evolution in our models. A consideration is whether a single snapshot of the field at a particular time is consistent with waves on decadal timescales; the field snapshot may actually contain features that are caused by torsional waves. In order to assess whether a snapshot or a time-averaged field should be used in the calculations, we compared the radial magnetic field at the CMB according to COV-OBS in three cases: a snapshot in 2010, a 50 year time-average (1960–2010), and a 130 year time-average (1840–2010). The three fields are very similar in both spatial structure and in amplitude, with only a few small length scale features vanishing from the 130 year average compared to the modern snapshot, see Fig. 2. Rather than small-scale features being absent from the field prior to 1960, it is likely that observational limitations and spatial coverage at the time were not sufficient to resolve them. From this, it seems that the choice between the two field

models, and between a snapshot of the radial field at the CMB and a time-averaged field, is unlikely to greatly influence the results. Therefore, we chose the 2010 radial field according to COV-OBS for our synthetic data production, anticipating that changes in the field over the wave model period, such as the westward drift and the relatively recent appearance of small length-scale features, would result in only minor changes to the wave-induced SV. As observationally-constrained field models describe the geomagnetic field above the core surface, and only up to degree 14 (e.g., Gillet et al. (2010)), such models provide no constraint on the profile of $\{B_s^2\}$ inside the core. Therefore, whilst there is no inconsistency between the $\{B_s^2\}$ profiles used in the forward models and the COV-OBS background magnetic field used for wave-induced SV calculations, the lack of observational constraints on the internal field is an inherent limitation of our forward models.

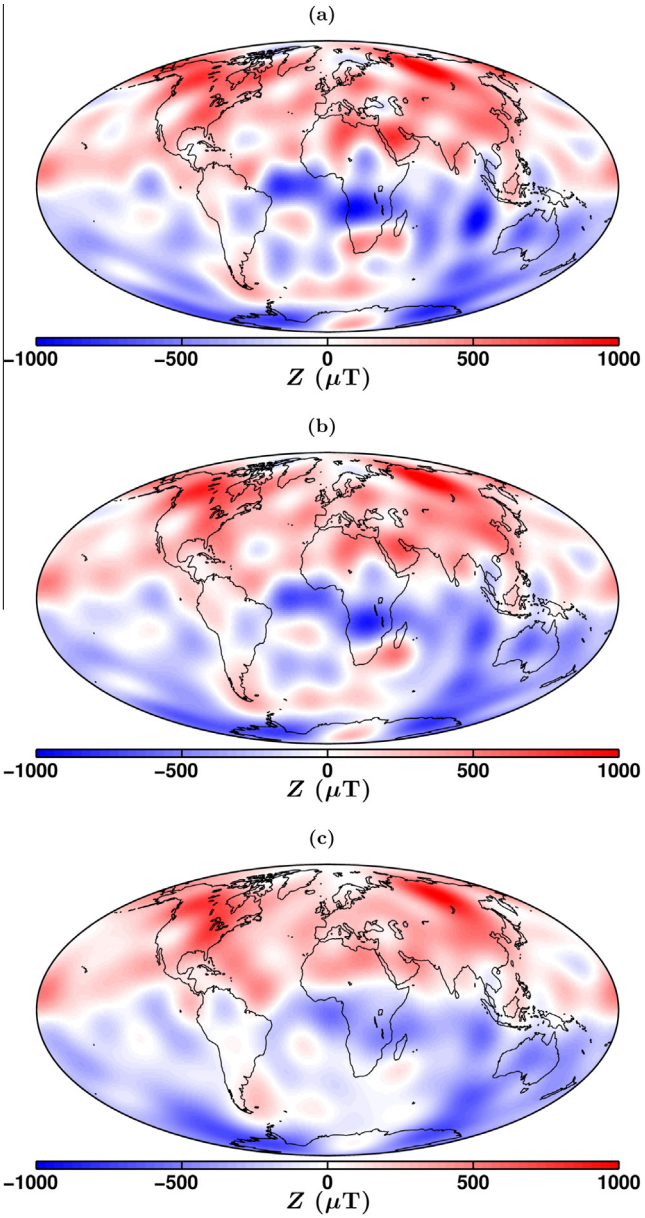

Fig. 2. The Z $(= -B_r)$ component of the geomagnetic field at the CMB according to the COV-OBS field model (Gillet et al., 2013) (a) snapshot of the field in 2010 (b) 50 year time-averaged field (1960–2010) and (c) 130 year time-averaged field (1840–2010). The scale is in μT; red indicates positive field (entering the core) and blue indicates negative field (exiting the core). (For interpretation of the references to color in this figure legend, the reader is referred to the web version of this article.)

3. Results

3.1. SV patterns: bulk rotation of core fluid

As Bloxham et al. (2002) noted in the first paper linking geomagnetic jerks to torsional oscillations, local magnetic field morphology dictates whether a particular location is sensitive to zonal core flow. This is an important point because some jerks are observed globally, while others are seen on regional scales, which has previously hindered identification of a common physical origin for these events. For a bulk rotation of the core fluid with respect to the mantle (constant ω_g), the SV obtained can be predicted from Eq. (4); differentiating the background B_r (from the field model) with respect to ϕ and multiplying by $-\omega_g$ (angular velocity, $\omega_g = u_\phi/s$) shows the pattern of SV that is expected to arise when all of the fluid in the core is perturbed equally, shown in Fig. 3a. This sensitivity test distinguishes between regions where the field at the CMB is sensitive to zonal core flow, and those unaffected by it. The red and blue regions show where zonal flow induces a signal in the SV, whilst the white areas indicate regions that are not sensitive to zonal flow because there are no azimuthal gradients in the radial field at that location. An interesting point is that the pattern is also very similar to the observed SV at the same time (see Fig. 3b), particularly in the equatorial Atlantic region,

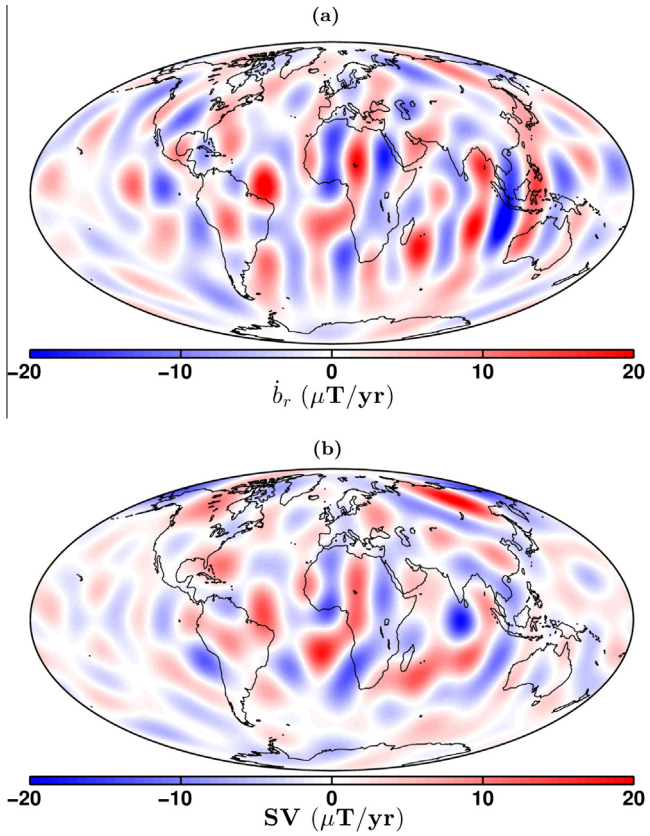

Fig. 3. (a) The radial SV at the CMB, $\dot{b}_r$, induced by the interaction of the field shown in Fig. 2(a) with a westward bulk rotation of the core fluid with respect to the mantle of ~0.3°/yr (b) the radial SV of the geomagnetic field at the CMB in 2010 according to the COV-OBS field model. The scale is in μT/yr; red indicates more positive field (more exiting the core) and blue indicates more negative field (more entering the core). (For interpretation of the references to color in this figure legend, the reader is referred to the web version of this article.)

which implies that much of the observed SV can be accounted for by a general zonal core flow. A westward bulk rotation of ∼0.3°/yr was needed to match the amplitudes of the observed SV, which corresponds to core flows of approximately 18 km/yr at the equator. The observed westward drift of the historical geomagnetic field at a rate of approximately 0.2°/yr has long been associated with a general westward flow at the top of the core (Bullard et al., 1950; Jackson, 1997; Jault et al., 1988; Dumberry and Finlay, 2007).

3.2. Synthetic SV time series: 'fast' torsional waves

As previously discussed, the torsional wave velocities u_ϕ must be scaled by an appropriate amplitude in order to produce time series and maps of torsional wave-induced SV; recall that the torsional wave equation has no intrinsic scale. Having chosen the internal magnetic field amplitude to give a core transit time of approximately 6 years in order to be consistent with the results of Gillet et al. (2010); Gillet et al. (2015), we chose to scale our fast torsional waves to match their amplitude as well. The torsional waves in that study had maximum amplitudes of approximately 0.4 km/yr. When this amplitude is used, the resulting SV is relatively small; the amplitudes of $\dot{x}$ and $\dot{y}$, the northwards and eastwards components respectively, are generally less than ±20 nT/yr at the CMB and the radial component, $\dot{z}$, is a factor of 2–3 larger. Fig. 4 shows the SV induced by the torsional waves of the forward model in the full sphere model of CLM.

The single pulse of the initial profile in Fig. 4a, which is placed at the midpoint of the core radius ($s = c/2$), manifests as two bands of SV at mid to high-latitudes. The location of these bands is equatorially symmetric due to the symmetry of the columnar flow comprising torsional waves, but the bands themselves are not equatorially symmetric because the local magnetic field morphology differs in the northern and southern hemispheres. The locations of the lines of zero wave-induced SV match those in Fig. 3a, which describe where the background magnetic field has no longitudinal variations and these differ in each hemisphere. After 1 year, the wave has split into two smaller pulses that begin to move away from the initial pulse position ($s = c/2$), see Fig. 4b. The two velocity pulses now manifest as four bands of SV, two at slightly lower latitudes than before and two at slightly higher latitudes than the initial bands. Fig. 4c shows the wave profile after 2 years when one pulse has moved towards the rotation axis and the other towards the equator of the CMB. Due to the geometry of torsional waves, the pulse near the rotation axis perturbs the magnetic field in the polar regions and the pulse near the equator of the CMB perturbs the field in equatorial regions. Fig. 4d shows the wave profile at 3 years, during the first reflections and phase shifts of the pulses. The strong SV in the equatorial region is due to the waves being high amplitude during the reflection at the stress-free boundary. The band is wider than in the previous figures because the wave is no longer a distinct pulse at the equator; at least the outermost 500 km of the core fluid is perturbed. The wave pulse near the rotation axis is smaller than before the phase shift and of the opposite polarity, which explains the sign reversal of the SV and lower amplitude signal. The SV signals are seen across the whole core surface as the wave becomes dispersed and the energy spreads

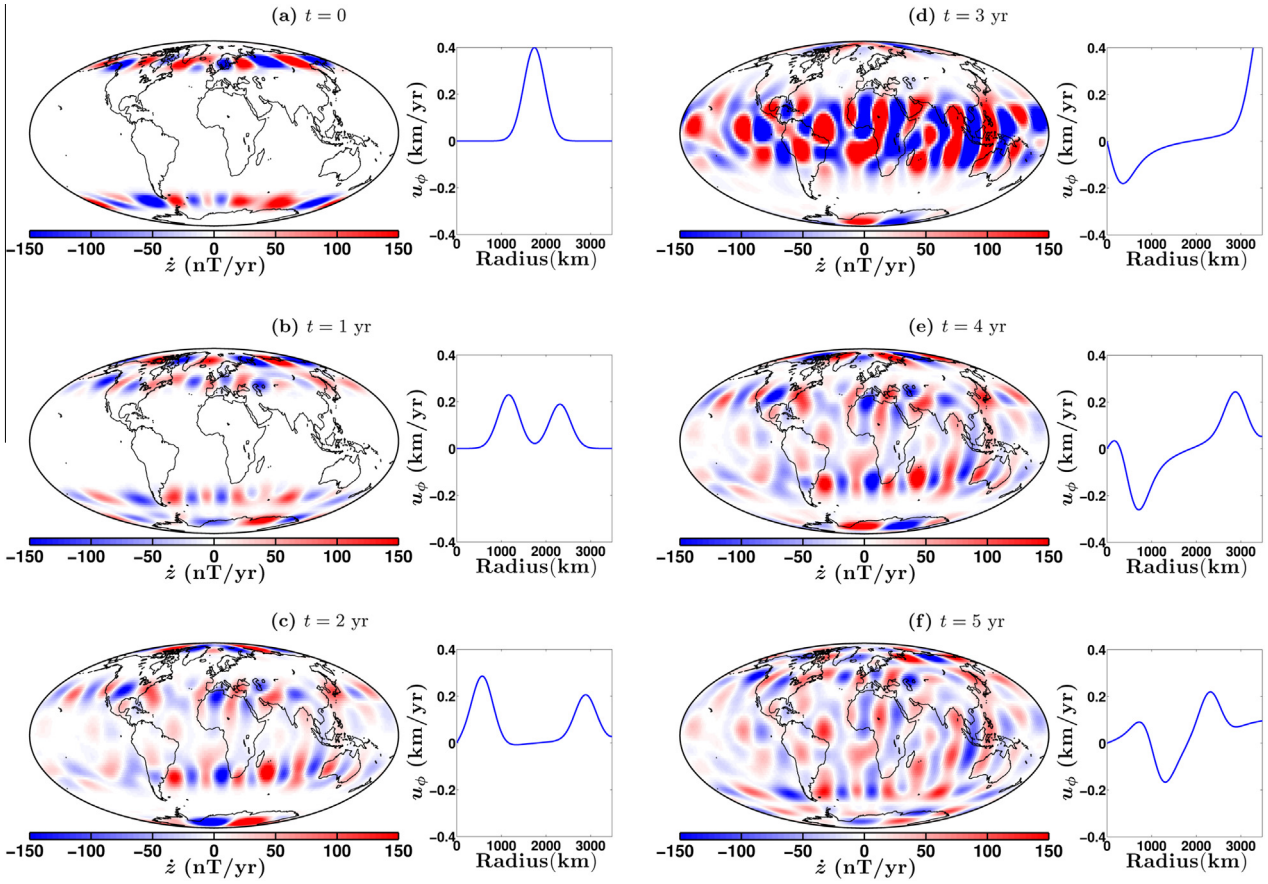

Fig. 4. Maps of the radial component of the SV induced by torsional waves with a 6 yr core transit time and an initial wave pulse amplitude of 0.4 km/yr. The maps are shown at 1 yr intervals, starting from the initial profile at $t = 0$ yr in (a) and ending at $t = 5$ yr in (f). The SV is evaluated at the CMB and the colour scale is from −150 nT/yr to 150 nT/yr. The torsional wave profile is shown on the right, with cylindrical radius (km) on the horizontal axis and zonal velocity (km/yr) on the vertical axis. (For interpretation of the references to color in this figure legend, the reader is referred to the web version of this article.)

through the domain, see Fig. 4e and f for the wave profiles and corresponding SV signals after 4 and 5 years respectively. The lines of zero wave-induced SV arise from two effects; first, the background field has no longitudinal variations in some locations and second, the velocity profile crosses $u_\phi = 0$ at several radii throughout the core, which results in no induced SV along certain bands of latitude.

As the dynamics of the waves in the forward models presented in CLM were very similar, we shall focus on the full sphere model in this paper; the effects of changing geometry to that of a spherical shell or adding a spatially varying $\{B_s^2\}$ profile would result in only minor differences in the SV maps. In CLM, we also considered the effect of wavelength on torsional wave propagation, finding that long wavelength features are more dispersive than short wavelength features, though the general dynamics of the modelled waves were very similar for all wavelengths. Increasing the wavelength of the initial pulse, by increasing the value of σ in (2), results in wider bands of SV because the wave occupies more of the core and perturbs a larger portion of the ambient magnetic field. Conversely, narrower initial pulses than that shown in Fig. 4a occupy less of the core and therefore perturb less of the magnetic field, resulting in narrower bands of SV. The amplitude of the SV is unchanged by varying the wavelength because it is determined only by the amplitude of the torsional wave.

Having examined the general structure of SV induced by torsional waves travelling through the core, it is now of interest to investigate the signals that would be observed at particular locations throughout wave evolution. Fig. 5 shows the locations of the 24 magnetic observatories at which synthetic SV time series were produced. These observatories are a sample of the total number of observatories worldwide and were chosen to give good global coverage. We first calculate the wave-induced SV at the CMB, using the real observatory latitudes and longitudes.

As previously discussed, all of the observatories record different SV signals, but all share two common traits: first, the amplitudes are quite small and second, the timescales are very short. Also, the predicted signals show some periodicity because the waves travel beneath the same location approximately every six years.

For example, Fig. 6a shows the signal predicted at the Bangui observatory in the Central African Republic, at CMB radius. At this station, the SV signals are relatively large compared to other stations, approximately 200 nT/yr, and vary on timescales of 6 yr due to the torsional wave periodicity imposed by the magnetic field strength. Fig. 6b shows that very little SV is predicted at the Eskdalemuir observatory in Scotland and Fig. 6c shows that the signal predicted at Niemegk in Germany also varies on the same timescale and reaches approximately half the amplitude as at Bangui. One of the objectives of this work was to investigate whether the torsional waves in our forward models produce signals that resemble geomagnetic jerks.

Of course, we do not observe jerks at the CMB, but at observatories on Earth's surface and via satellite observations. The syn-

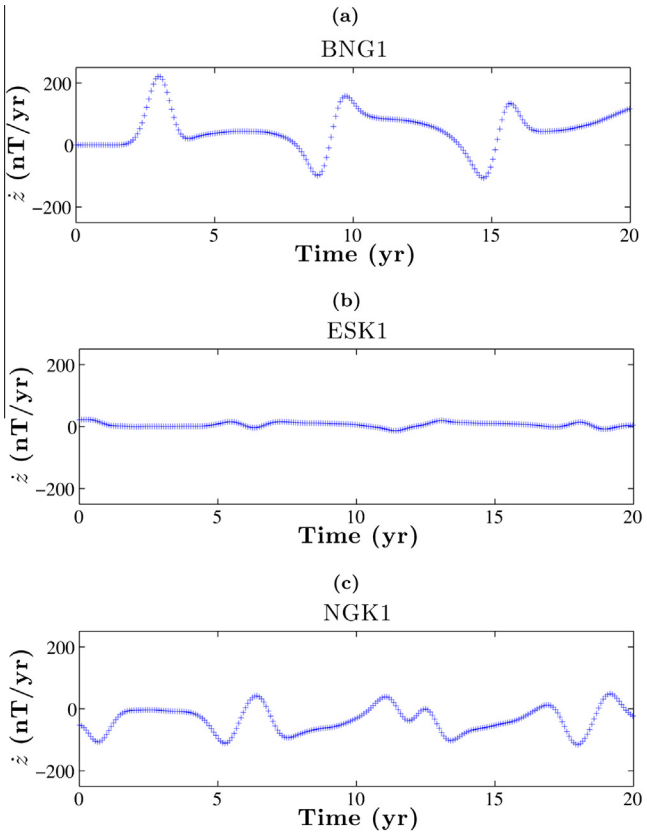

Fig. 6. Time series of the z component of the SV induced at the CMB by torsional waves with a 6 yr core transit time and an initial pulse amplitude of 0.4 km/yr at (top) Bangui, (middle) Eskdalemuir and (bottom) Niemegk.

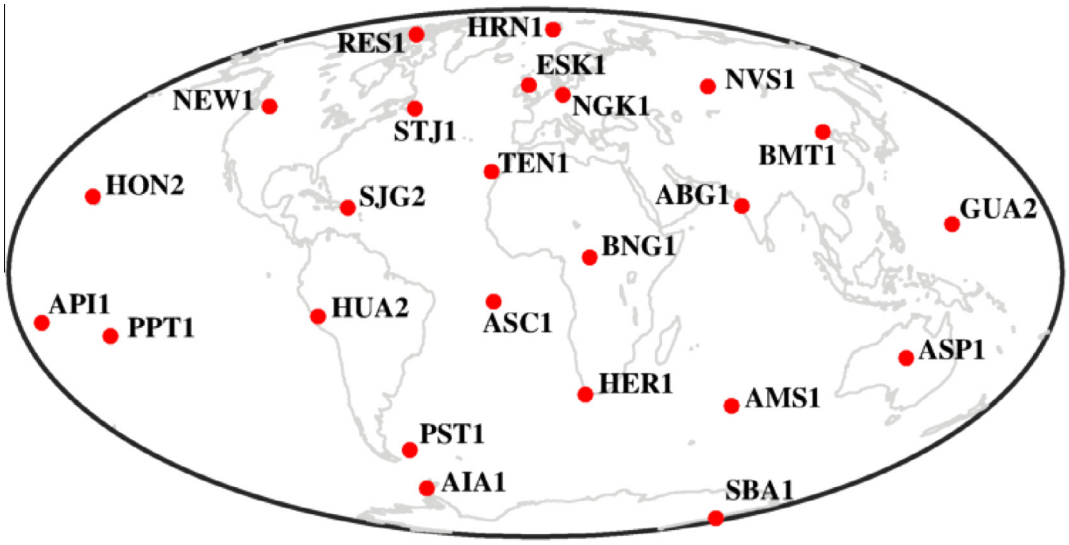

Fig. 5. The locations of the 24 magnetic observatories at which synthetic time series of wave-induced SV will be produced.

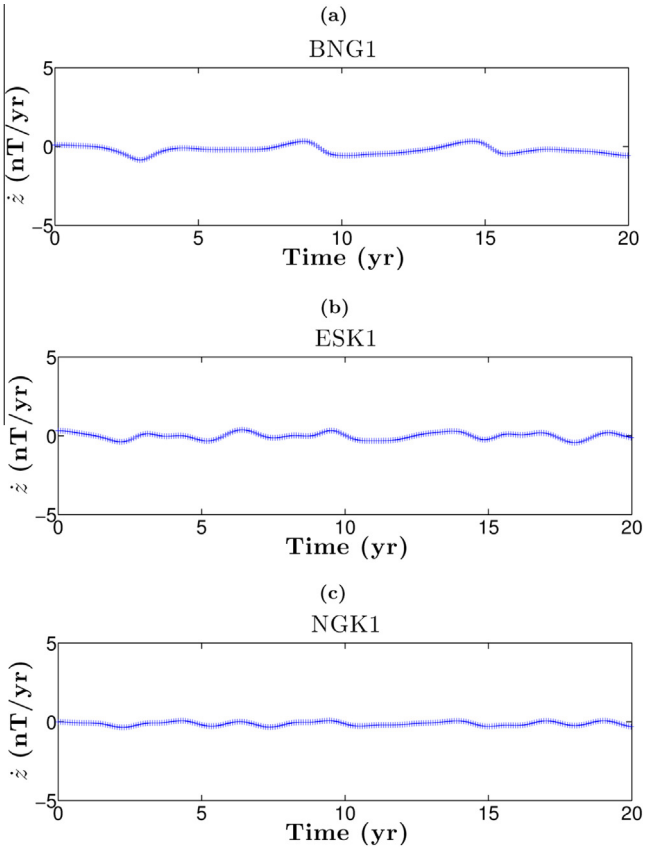

Fig. 7. Time series of the *z* component of the SV induced at Earth's surface by torsional waves with a 6 yr core transit time and an initial pulse amplitude of 0.4 km/yr at (top) Bangui, (middle) Eskdalemuir and (bottom) Niemegk.

thetic SV time series were upward continued, using spherical harmonic coefficients, to the Earth's surface (taken as 6371 km) in order to permit comparison with magnetic data, see Fig. 7. Note rapid timescales of the signals and very small amplitudes (<3 nT/yr) compared to the typical magnitudes of observed SV (a few tens of nanotesla at Earth's surface, (Matzka et al., 2010) and Fig. 8), and the maximum amplitudes of SV predicted by observationally-constrained field models (approximately 200 nT/yr, see, among others, the *gufm1* (Jackson et al., 2000), COV-OBS (Gillet et al., 2013) and CHAOS-4 (Olsen et al., 2014) models).

We applied the jerk detection method of (Brown et al., 2013), based on the method of Pinheiro et al. (2011), to the synthetic time series evaluated at Earth's surface. It identifies jerks by applying a two-part linear regression to a sliding window of a single component of observatory SV data and generating a probability density function (PDF) of the 'likeliness' of potential jerk occurrence times. A potential jerk occurrence is considered at each time step as the linear regression is iterated across the window of data, and the misfit of the regression to the data is used to build the PDF. The summation of the resulting overlapping probability functions is then normalised to an integral of 1, so as to produce a continuous PDF for the entire series of data under consideration. The modified method uses the same procedure for estimating time uncertainties as described in Pinheiro et al. (2011), but Brown et al. (2013) introduced a threshold probability above which an event may be considered 'significantly likely' compared to the background level of 'likeliness' that arises from the misfit of the regression to the variability in the data. Brown et al. (2013) also require a minimum jerk amplitude below which an event is not considered significant compared to the background noise level of the data.

For consistency, we used the same parameters on the synthetics as Brown et al. (2013) used on the real magnetic data for the period 1958–2008. These parameters include a PDF threshold cut-off (taken as 0.2 in Brown et al. (2013), based on trade-off curve of

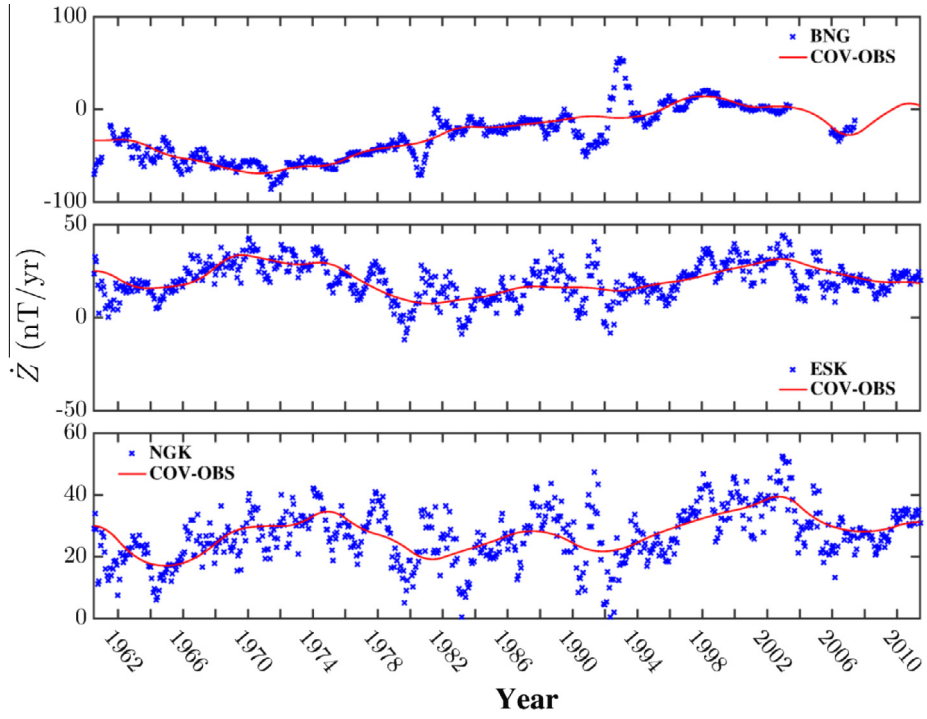

Fig. 8. Time series of the *z* component of the SV observed at Earth's surface during the period 1960–2010 at (top) Bangui, (middle) Eskdalemuir and (bottom) Niemegk.

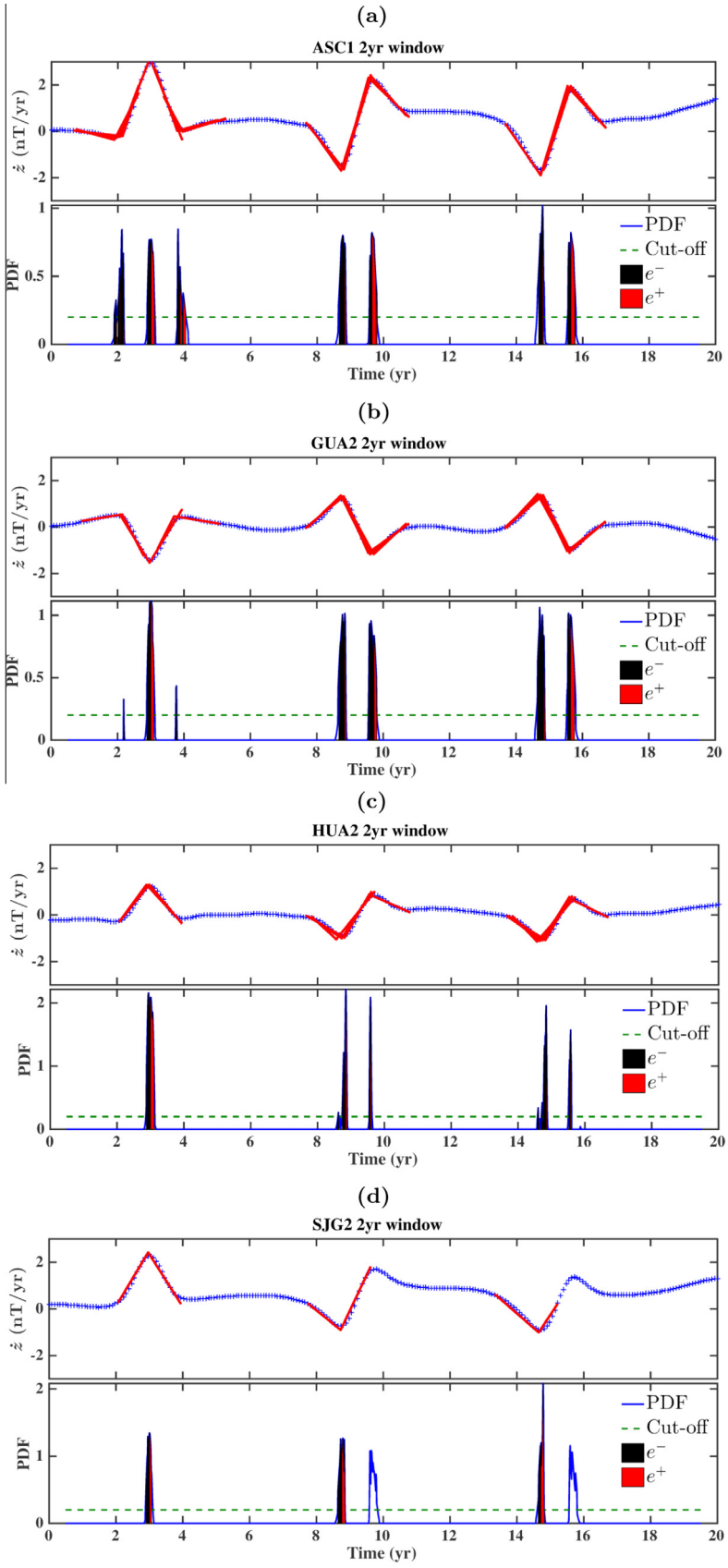

Fig. 9. The top panel of these figures shows a time series of a single component of the SV signal (in nT/yr) at (a) Ascension Island, (b) Guam, (c) Huancayo and (d) San Juan throughout the 20 years of the torsional wave forward model. The observatory name and window length are displayed at the top of each subfigure, and identified jerk events are shown as a red 'V' shape fitted to the SV series. The bottom panel shows the calculated PDF from the two-part linear regression, with the chosen threshold cut-off value of 0.2 shown as a green line. The positive and negative errors on the PDF are filled in underneath the PDF curve in red and black, respectively. (For interpretation of the references to color in this figure legend, the reader is referred to the web version of this article.)

the number of jerks detected versus the probability cut-off threshold above which peaks in probability are considered jerks), a minimum jerk amplitude (3 nT/yr^2) and the window length for the linear regression. Four different window lengths (5, 10, 15 and 20 yr) were applied to each individual component of the SV time series, and a two-part linear regression was fitted to the series at every potential jerk occurrence time (taken at intervals of 0.001 yr so as to be smaller than the monthly (0.08 yr) synthetic

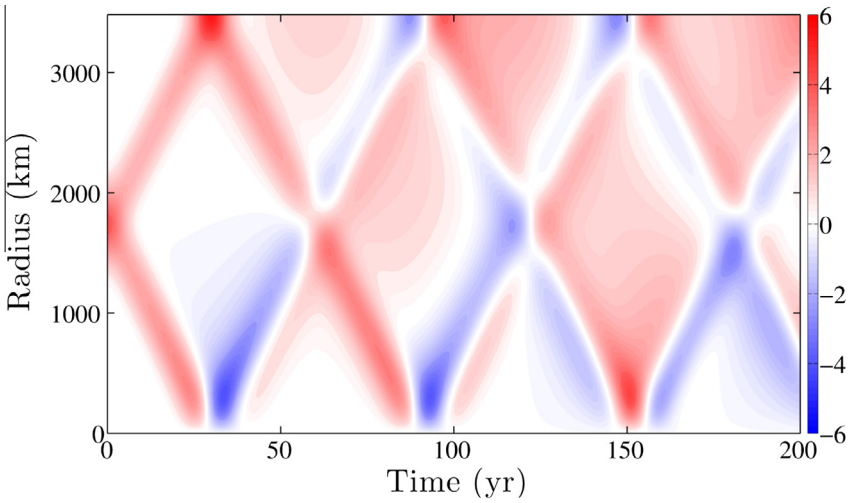

Fig. 10. Contour plot of the velocity u_ϕ of torsional waves in a full sphere, with time on the horizontal axis and cylindrical radius on the vertical axis. Red corresponds to positive velocity and blue corresponds to negative velocity. The colour scale is from −6 km/yr to 6 km/yr; the initial wave pulse had an amplitude of 4 km/yr and the waves have a 60 yr core transit time. (For interpretation of the references to color in this figure legend, the reader is referred to the web version of this article.)

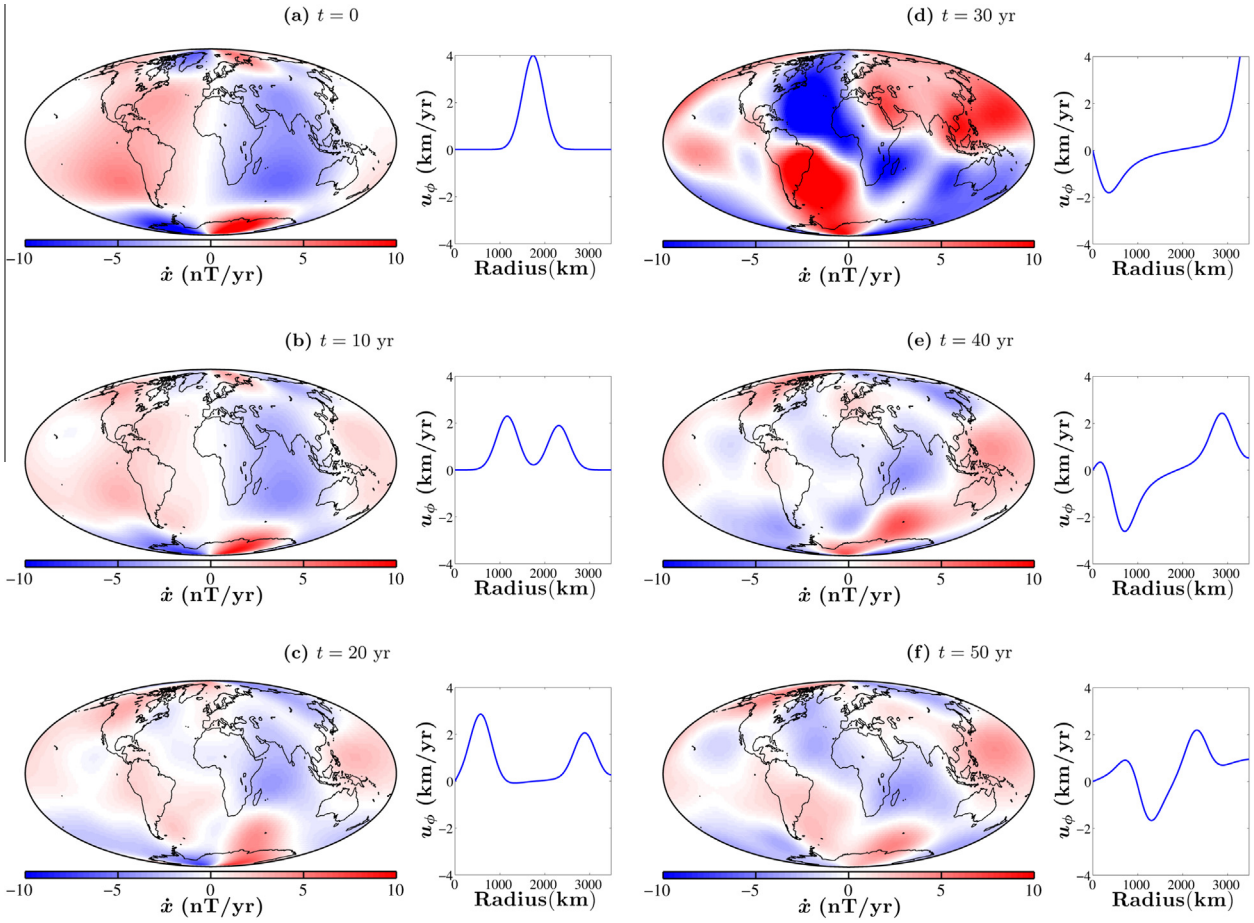

Fig. 11. Maps of the x component of the SV induced by torsional waves with a 60 yr core transit time and an initial wave pulse amplitude of 4 km/yr. The maps are shown at 10 yr intervals, starting from the initial profile at $t = 0$ yr in (a) and ending at $t = 50$ yr in (f). The SV is evaluated at the Earth's surface and the colour scale is from −10 nT/yr to 10 nT/yr. The torsional wave profile is shown on the right, with cylindrical radius (km) on the horizontal axis and zonal velocity (km/yr) on the vertical axis. (For interpretation of the references to color in this figure legend, the reader is referred to the web version of this article.)

data sampling). No synthetic jerks were identified in our modelled SV with these parameters, in particular, the window lengths were much too long for the inherent timescales of the modelled signals. Jerks in real SV data generally consist of two linear segments of data that are several years (or decades) long, with the jerk event being the very rapid (<1 yr) change from one gradient to the other. In the synthetics, the SV does change slope very rapidly in many of the time series but these changes do not separate long periods of SV of constant slope; the rapid changes are bracketed by linear SV segments of only a few months and, often, two rapid changes occur in quick succession due to the wave passing beneath a particular location and then changing direction, after reflection for example, and passing beneath the same point again shortly afterwards (Fig. 7). In order to identify jerk-like signals in the synthetics evaluated at Earth's surface, the jerk algorithm required very short sliding windows (<2 yr) and the signals identified were the very rapid 'wiggles' described above.

Fig. 9 shows some results of applying the jerk algorithm to the SV predicted by fast torsional waves at four different observatories. These observatories were Ascension Island (ASC1), Guam (GUA2), Huancayo, Peru (HUA2) and San Juan, Puerto Rico (SJG2). The top panel of the jerk results figures shows a time series of a single component of the SV signal (in nT/yr) at a particular observatory throughout the 20 years of the torsional wave forward model. The observatory name and the window length are displayed at the top of each figure, and any identified jerk events are shown as a red 'V' shape fitted to the synthetic SV series. The bottom panel shows the calculated PDF from the two-part linear regression, with the chosen threshold cut-off value shown as a green line. Assuming Gaussian error distributions about the peaks in likeliness, estimates of the uncertainties in the occurrence times and in jerk amplitudes were calculated; the positive and negative uncertainties on the PDF are filled in underneath the PDF curve in red and black respectively. As described by Brown et al. (2013), the PDF values are normalised to a value of one across the entire window to account for any jerk events being identified in several windows during the sliding regression. Note that for narrow PDF curves, the values of the PDF are high (>1) because the algorithm normalises the area of a spike. Using the wave amplitude and timescales of Gillet et al. (2010), we must conclude that our 'fast' torsional waves do not produce jerk-like signals because the timescales of the synthetic SV are much too rapid and the signals are too small at Earth's surface (the largest are less than 3 nT/yr). In addition to being smaller than the observed SV at many observatories (Fig. 8), it is unclear whether the modelled signals, typically 1–2 nT/yr, could be resolved in geomagnetic data (SV observatory data are generally accurate to 0.5–2 nT/yr (Reda et al., 2011)).

3.3. Synthetic SV time series: 'slow' torsional waves

The waves described in the previous section propagated much faster those in previous studies and of relatively small amplitude, which raises the question of whether matching torsional waves in other studies might yield results that bear more resemblance to real SV data. Based on previously determined torsional oscillation periods (discussed in Section 1), a forward model of torsional waves with a revised core transit time and wave amplitude was run, Fig. 10. The amplitude of the initial wave pulse was set to

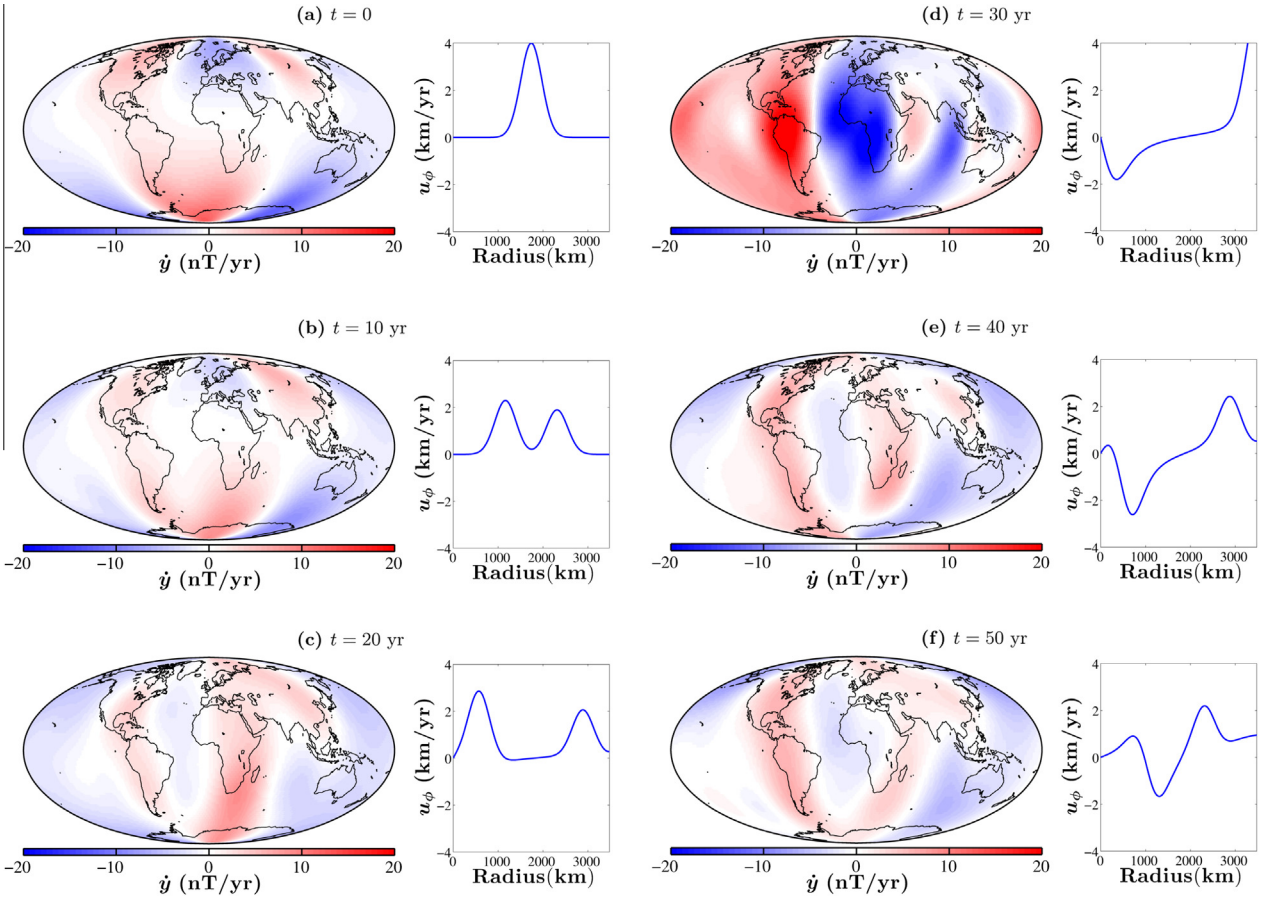

Fig. 12. As for Fig. 11, but for the $\dot{y}$ component. The colour scale is from −20 nT/yr to 20 nT/yr. (For interpretation of the references to color in this figure legend, the reader is referred to the web version of this article.)

4 km/yr, for consistency with previously determined torsional wave amplitudes (e.g., Zatman and Bloxham (1997)) and the core transit time was 60 yr. Having rescaled our torsional wave timescales and amplitudes, by increasing the amplitude term in Eq. (2) and decreasing the magnitude of $\{B_s^2\}$, we produced synthetic time series of the induced SV at the previously discussed observatories. The spatial SV patterns at the CMB are the same as discussed in the previous section, but the temporal scales are now elongated compared to the previous model. As seen in Fig. 4, much of the wave-induced SV is small length scale at the CMB. At Earth's surface, the small length scale features of the induced SV have been attenuated during the upward continuation and the majority of the SV is of degree $l < 5$. This filtering out of small length scales would be increased in the case of the mantle containing any electrically conducting material. This screening by conductive material is an effect that is typically neglected in models (though see Pinheiro and Jackson (2008) for a study relating mantle electrical conductivity and jerk differential time delays), but the presence of such material is thought likely for parts of Earth's lower mantle (e.g., Shankland et al. (1993)).

Maps of the x, y and z components of the torsional wave-induced SV at six different times during the first core transit time are shown in Figs. 11–13.

The magnitudes of the synthetic SV are an order of magnitude larger than in the previous 'fast' waves model, due to the increased torsional wave amplitude, and all three components are large enough to be resolved in observations (see Figs. 1 and 8, the amplitude of the observed SV at the Earth's surface (~ 200 nT/yr) and Wardinski and Holme (2011) and Brown et al. (2013)).

The jerk detection method identified several jerk events at Earth's surface, Fig. 15a. As discussed for the fast transit time waves, the signals retain some periodicity due to waves travelling beneath some locations at set intervals. This periodicity results in several successive jerks being observed at some observatories, but there is only weak evidence for such periodic jerks in real magnetic data (Brown et al., 2013). In general, the identified jerk events occurred in single components of the SV and were localised to small regions. Since the torsional waves perturb the ambient magnetic field in two equatorially symmetric bands of latitude, the waves do not generally produce signals that are observed everywhere at the same time, though more observatories see signals simultaneously towards the end of the wave model because the wave energy has dispersed through the domain. However, these signals tend to be low amplitude and smoothly varying. At $t = 30$ yr, an SV signal is predicted in all three components at most observatories due to the high torsional wave amplitudes during reflection from the stress-free CMB (see Figs. 11d, 12d and 13d). Note that many of the signals identified by the jerk algorithm occur around the reflection time (see Fig. 14 for a few examples and the red box in Fig. 15a). Such large-scale, contemporaneous SV signals are consistent with, for example, the global jerk event observed in 1969 (Courtillot et al., 1978; Malin et al., 1983; Whaler, 1987).

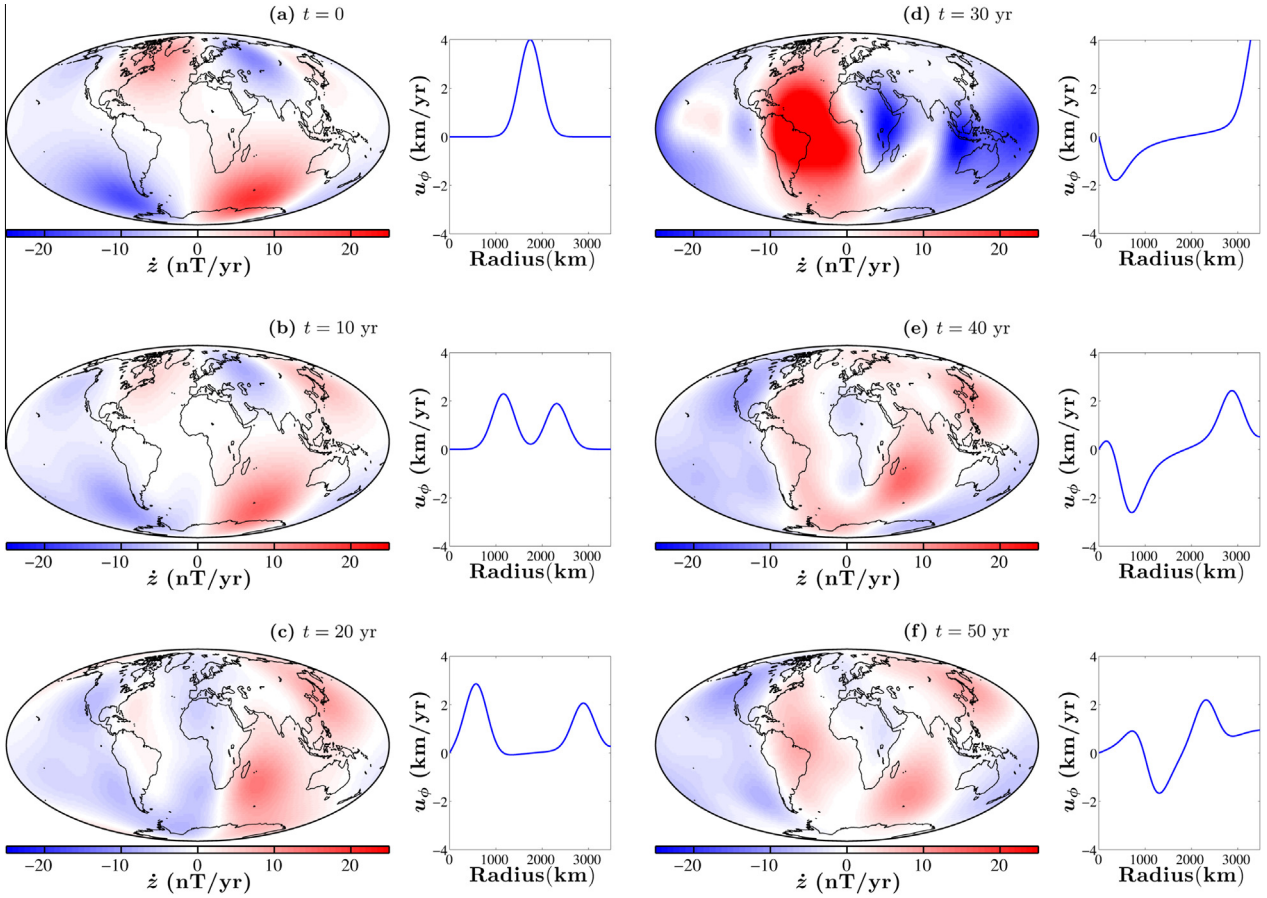

Fig. 13. As for Fig. 11, but for the $\dot{z}$ component. The colour scale is from −20 nT/yr to 20 nT/yr. (For interpretation of the references to color in this figure legend, the reader is referred to the web version of this article.)

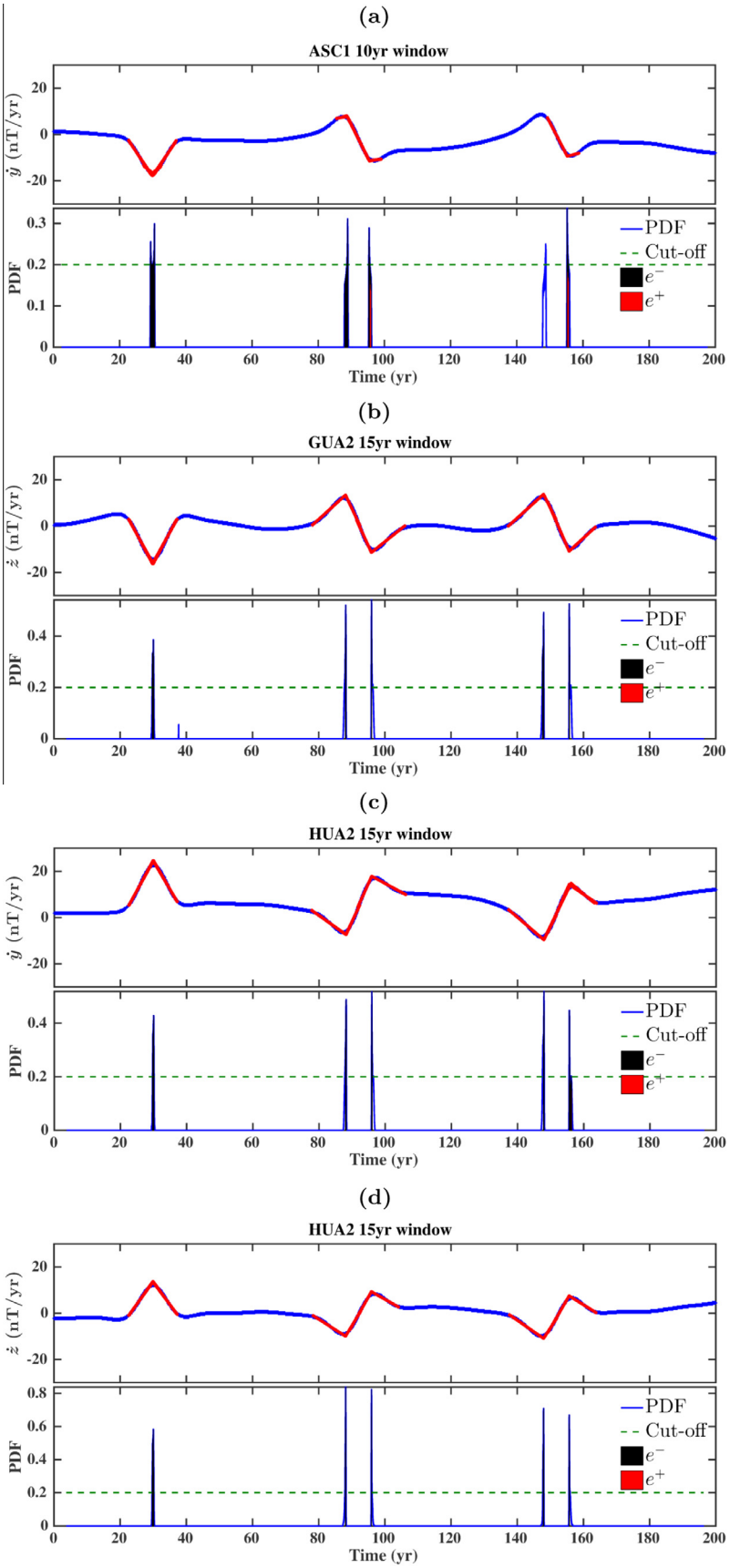

Fig. 14. As for Fig. 9, but for the slow transit time torsional waves shown in Fig. 10.

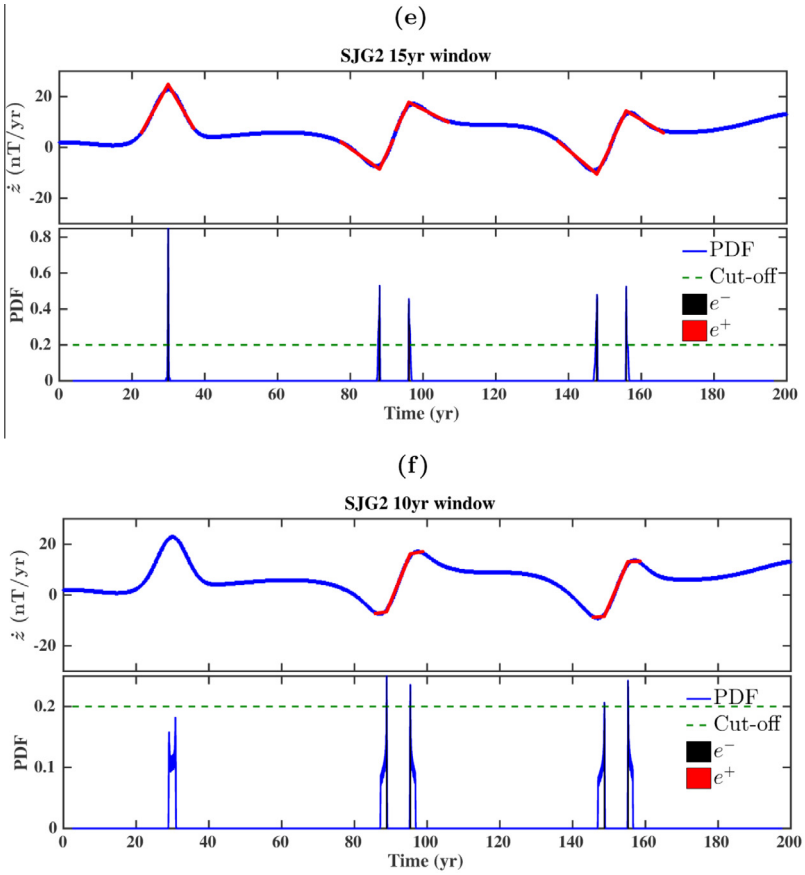

Fig. 14 (*continued*)

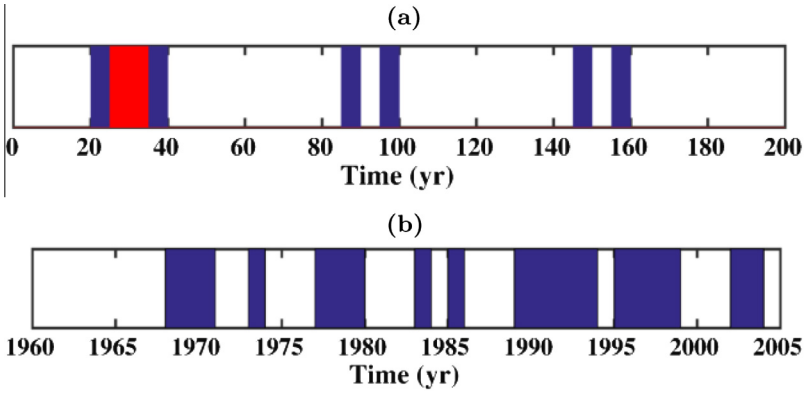

Fig. 15. (a) Summary of identified jerk occurrences for SV generated by slow torsional waves. Blue boxes represent jerks that are identified in any component at one or more of the 24 observatories shown in Fig. 5 (i.e. 'local' jerk events). The red box shows the time of the 'global' jerk event that takes place as the waves reflect from the equator of the CMB. (b) Summary of the jerk events identified in Brown et al. (2013) and references therein. (For interpretation of the references to color in this figure legend, the reader is referred to the web version of this article.)

4. Discussion and conclusions

We have used the induction equation under the frozen flux assumption and velocities from torsional wave forward models to produce synthetic maps and time series of wave-induced SV. The required background fields were taken from the COV-OBS model of Gillet et al. (2013), though using different field models and/or time-averaged fields gave equivalent results. We conducted a sensitivity test of the magnetic field to a bulk rotation of the core fluid, finding that global zonal core flows produce SV signals that strongly depend on the local magnetic field morphology and in particular, on the field's longitudinal variations. As Bloxham et al. (2002) noted, the local effects of field structure may explain why some jerk events are only observed on regional scales and implies that small length scale core flow need not necessarily be the cause of regional SV signals. However, some geomagnetic jerks, such as the event in 1969, were observed at a global scale (Courtillot et al., 1978; Malin et al., 1983; Whaler, 1987), but not all parts of Earth's magnetic field are sensitive to zonal core flows at any particular time. Since torsional waves (or other zonal flow) do not generally produce global contemporaneous SV signals (though see the above discussion of the SV signal during wave reflection at the

CMB), we concur with previous studies (e.g., Wardinski et al. (2008) and Silva and Hulot (2012)) that suggested geomagnetic jerks cannot be caused by zonal flows alone, although such flows could be an important contributor to the observed SV. An interesting point to note from the sensitivity test is that the observed SV and that induced by a bulk rotation of the core fluid are remarkably similar, particularly in the equatorial regions. The amplitude of the bulk rotation required to match the observed SV amplitudes was approximately 0.3°/yr, which is similar to many estimates of the rate of westward drift of the geomagnetic field in the equatorial Atlantic (e.g., Bullard et al., 1950; Jault et al., 1988; Dumberry and Finlay, 2007).

We set out to investigate whether the torsional waves in our forward models can produce SV signals that resemble geomagnetic jerks. Several studies have linked the origin of jerks to torsional oscillations and/or toroidal core flows (e.g., Waddington et al., 1995; Bloxham et al., 2002; Olsen and Mandea, 2008; Wardinski et al., 2008; Silva and Hulot, 2012). We considered two different scaling for torsional waves: 'fast', low amplitude waves and 'slow', high amplitude waves. When the wave amplitudes and timescales are chosen to match a recent study of the 6 yr signal in ΔLOD by Gillet et al. (2010), the resulting SV signals were very small (<3 nT/yr at Earth's surface). The timescales of the induced SV signals are very short, due to the 6 yr core transit time, and are consequently too rapid to be considered as jerks. However, torsional oscillations have most often been linked to decadal signals in geophysical data with higher amplitudes (e.g., Braginsky, 1970; Zatman and Bloxham, 1997, 1999; Hide et al., 2000; Roberts et al., 2007; Dickey and de Viron, 2009), and so we recalculated the SV signals induced by slow torsional waves with a 60 yr core transit time and an increased amplitude of 4 km/yr.

We applied the jerk detection method of Brown et al. (2013) to the synthetic SV series evaluated at Earth's surface, using the same parameters as they used on real magnetic data. Various signals were identified as jerks in the synthetic data, though they do not appear to resemble SV signals that have traditionally been identified as jerks. At all observatories, the SV signals are smoothly-varying and do not resemble the sharp 'V' shape that is usually associated with geomagnetic jerks. However, despite the prevalence of this definition, not all authors agree that jerks should be defined as sharp changes in SV (e.g., Alldredge, 1984, 1985). Demetrescu and Dobrica (2005, 2014) decomposed the geomagnetic field variation into its multidecadal ingredients, which include a 'steady variation' and three quasi-periodic signals of ∼11 yr, ∼22 yr and ∼80 yr. They found that jerks arise from the combination of the internal 22 yr and 80 yr signals, which is consistent with several other authors who favour an internal origin for jerks (e.g., Malin and Hodder, 1982). Demetrescu and Dobrica (2014) further proposed that since jerks are caused by smoothly-varying periodic signals, they are not inherently sharp SV signals and that contamination by the external 11 yr signal causes the often reported 'V' shape on very short timescales, and also influences the amplitude and timing of the jerk. The smoothly varying SV signals induced by our torsional waves seem to be more consistent with the results of Demetrescu and Dobrica (2005, 2014) than other studies requiring sharp SV variations.

Many of the signals in our models are only identified in a single component of the field, and several jerks often occur in quick succession due to the periodic propagation of waves under particular locations. Despite attempts by Brown et al. (2013), such periodicities have not been identified in jerk occurrences in observatory data. The timings of real jerk occurrences may be linked to sudden changes in time rate of changes in length-of-day (LOD) (e.g., Holme and de Viron, 2013; Olsen and Mandea, 2007; Mandea et al., 2010), to changes in the phase of the Chandler wobble (e.g., Bellanger et al., 2001, 2002; Gibert and Le Mouël, 2008) and to changes in the phase of the free core nutation (Shirai et al., 2005; Malkin, 2013). These correlations suggest a common underlying physical phenomenon that involves both core flow and angular momentum exchanges with the mantle, such as torsional waves. If torsional waves in the core are related to geomagnetic jerks, it could be that the waves are generated in one region of the core, the tangent cylinder for example (Livermore and Hollerbach, 2012; Teed et al., 2015), and are damped out in another region so that the waves do not reflect from the core boundaries (Schaeffer et al., 2012). If the base of the lower mantle were electrically conducting, the waves would likely be rapidly attenuated at the top of the core (e.g., Dumberry and Mound (2008)) and so would be unable to produce the periodic signals seen in our forward models. Despite several suggestions, the excitation mechanism of torsional waves in the core has not yet been confirmed. The waves could be continually generated, periodically generated or irregularly generated, depending on the physical processes that excites them, and each of these scenarios would result in very different SV signals. In any case, our models of geomagnetic jerks favour 'slow' torsional waves, with core transit times of several decades so that jerk signals punctuate long time series of steady SV, and with amplitudes of at least 4 km/yr so as to produce signals on a similar scale to those recorded at magnetic observatories.

Acknowledgements

The authors gratefully acknowledge the input of Prof. Steve Tobias, whose insight and expertise greatly assisted this research. We also wish to thank Will Brown for the use of his jerk detection code and for many helpful discussions. This work was supported by NERC Grant NE/I012052/1.

Appendix A. Supplementary data

Supplementary data associated with this article can be found, in the online version, at http://dx.doi.org/10.1016/j.pepi.2016.03.012.

References

Alexandrescu, M., Gibert, D., Hulot, G., Le Mouël, J.L., Saracco, G., 1996. Worldwide wavelet analysis of geomagnetic jerks. J. Geophys. Res.: Solid Earth 101, 21975–21994. http://dx.doi.org/10.1029/96JB01648.
Alldredge, L.R., 1984. A discussion of impulses and jerks in the geomagnetic field. J. Geophys. Res.: Solid Earth (1978–2012) 89, 4403–4412.
Alldredge, L.R., 1985. More on the alleged 1970 geomagnetic jerk. Phys. Earth Planet. Int. 39, 255–264.
Backus, G., 1968. Kinematics of geomagnetic secular variation in a perfectly conducting core. Philos. Trans. Roy. Soc. Lond. A 263, 239–266.
Bellanger, E., Le Mouël, J.L., Mandea, M., Labrosse, S., 2001. Chandler wobble and geomagnetic jerks. Phys. Earth Planet. Inter. 124, 95–103.
Bellanger, E., Gibert, D., Le Mouël, J.L., 2002. A geomagnetic triggering of Chandler wobble phase jumps? Geophys. Res. Lett. 29, pp. 28-1.
Bloxham, J., Zatman, S., Dumberry, M., 2002. The origin of geomagnetic jerks. Nature 420, 65–68.
Braginsky, S.I., 1970. Torsional magnetohydrodynamic vibrations in the Earth's core and variations in the length of day. Geomag. Aeron. 10, 1–10.
Braginsky, S.I., 1984. Short-period geomagnetic secular variation. Geophys. Astrophys. Fluid Dyn. 30, 1–78.
Braginsky, S.I., 1999. Dynamics of the stably stratified ocean at the top of the core. Phys. Earth Planet. Int. 111, 21–34.
Brown, W., Mound, J., Livermore, P., 2013. Jerks abound: an analysis of geomagnetic observatory data from 1957 to 2008. Phys. Earth Planet. Inter. 223, 62–76. http://dx.doi.org/10.1016/j.pepi.2013.06.001, sI: 13th SEDI conference.
Buffett, B., 2014. Geomagnetic fluctuations reveal stable stratification at the top of the Earth's core. Nature 507, 484–487.
Buffett, B.A., Mound, J., Jackson, A., 2009. Inversion of torsional oscillations for the structure and dynamics of Earth's core. Geophys. J. Int. 177, 878–890.
Bullard, E.C., Freedman, C., Gellman, H., Nixon, J., 1950. The Westward drift of the Earth's magnetic field. Philos. Trans. Roy. Soc. Lond. A 243, 67–92.
Canet, E., Fournier, A., Jault, D., 2009. Forward and adjoint quasi-geostrophic models of the geomagnetic secular variation. J. Geophys. Res. 114, B11101.

Courtillot, V., Ducruix, J., Le Mouël, J., 1978. Sur une accélération récente de la variation séculaire du champ magnétique terrestre. CR Acad. Sci. D 287, 1095–1098.
Cox, G.A., Livermore, P.W., Mound, J.E., 2014. Forward models of torsional waves: dispersion and geometric effects. Geophys. J. Int. 196, 1311–1329. http://dx.doi.org/10.1093/gji/ggt414.
Davies, C.J., Gubbins, D., Jimack, P.K., 2011. Scalability of pseudospectral methods for geodynamo simulations. Concurrency Comput.: Pract. Exp. 23, 38–56. http://dx.doi.org/10.1002/cpe.1593.
Davis, R.G., Whaler, K.A., 1997. The 1969 geomagnetic impulse and spin-up of the Earth's liquid core. Phys. Earth Planet. Int. 103, 181–194.
Demetrescu, C., Dobrica, V., 2005. Recent secular variation of the geomagnetic field. New insights from long series of observatory data. Rev. Roum. Geophys. 49, 22–33.
Demetrescu, C., Dobrica, V., 2014. Multi-decadal ingredients of the secular variation of the geomagnetic field. Insights from long time series of observatory data. Phys. Earth Planet. Int. 231, 39–55.
Desjardins, B., Dormy, E., Grenier, E., 2001. Instability of Ekman–Hartmann boundary layers, with application to the fluid flow near the core–mantle boundary. Phys. Earth Planet. Inter. 123, 15–26.
Dickey, J.O., de Viron, O., 2009. Leading modes of torsional oscillations within the Earth's core. Geophys. Res. Lett. 36.
Dumberry, M., Finlay, C.C., 2007. Eastward and westward drift of the Earth's magnetic field for the last three millennia. Earth Planet. Sci. Lett. 254, 146–157.
Dumberry, M., Mound, J.E., 2008. Constraints on core–mantle electromagnetic coupling from torsional oscillation normal modes. J. Geophys. Res. 113, B03102.
Elsasser, W., 1946. Induction effects in terrestrial magnetism I. Phys. Rev. 69, 106–116.
Gibert, D., Le Mouël, J.L., 2008. Inversion of polar motion data: Chandler wobble, phase jumps, and geomagnetic jerks. J. Geophys. Res.: Solid Earth 1978–2012, 113.
Gillet, N., Pais, M., Jault, D., 2009. Ensemble inversion of time-dependent core flow models. Geochem. Geophys. Geosyst. 10.
Gillet, N., Jault, D., Canet, E., Fournier, A., 2010. Fast torsional waves and strong magnetic field within the Earth's core. Nature 465, 74–77.
Gillet, N., Jault, D., Finlay, C.C., Olsen, N., 2013. Stochastic modeling of the Earth's magnetic field: inversion for covariances over the observatory era. Geochem. Geophys. Geosyst. 14, 766–786. http://dx.doi.org/10.1002/ggge.20041.
Gillet, N., Jault, D., Finlay, C., 2015. Planetary gyre, time-dependent eddies, torsional waves and equatorial jets at the Earth's core surface. J. Geophys. Res.: Solid Earth.
Golub, G.H., Welsch, J.H., 1969. Calculation of Gauss quadrature rules. Math. Comput. 23, 221–230.
Gubbins, D., Davies, C., 2013. The stratified layer at the core–mantle boundary caused by barodiffusion of oxygen, sulphur and silicon. Phys. Earth Planet. Inter. 215, 21–28.
Gubbins, D., Tomlinson, L., 1986. Secular variation from monthly means from Apia and Amberley magnetic observatories. Geophys. J. Int. 86, 603–616.
Helffrich, G., Kaneshima, S., 2013. Causes and consequences of outer core stratification. Phys. Earth Planet. Inter. 223, 2–7.
Hide, R., Boggs, D.H., Dickey, J.O., 2000. Angular momentum fluctuations within the Earth's liquid core and torsional oscillations of the core–mantle system. Geophys. J. Int. 143, 777–786.
Holme, R., 2015. Large-scale flow in the core. In: Schubert, G. (Ed.), Treatise on Geophysics, 8. 91–113.
Holme, R., de Viron, O., 2013. Characterization and implications of intradecadal variations in length of day. Nature 499, 202–204.
Holme, R., Whaler, K., 2001. Steady core flow in an azimuthally drifting reference frame. Geophys. J. Int. 145, 560–569.
Jackson, A., 1997. Time-dependency of tangentially geostrophic core surface motions. Phys. Earth Planet. Int. 103, 293–311.
Jackson, A., Bloxham, J., Gubbins, D., 1993. Time-dependent flow at the core surface and conservation of angular momentum in the coupled core–mantle system. Dynamics of Earth's Deep Interior and Earth Rotation, 72. 97–107.
Jackson, A., Jonkers, A.R.T., Walker, M.R., 2000. Four centuries of geomagnetic secular variation from historical records. Philos. Trans. Roy. Soc. Lond. A 358, 957–990.
Jault, D., Légaut, G., 2005. Alfvén waves within the Earth's core. In: Jones, C.A., Hughes, D.H., Weiss, N.O. (Eds.), Fluid Dynamics and Dynamos in Astrophysics and Geophysics, The Fluid Mechanics of Astrophysics and Geophysics. CRC Press, pp. 277–293.
Jault, D., Le Mouël, J., 1991. Physical properties at the top of the core and core surface motions. Phys. Earth Planet. Inter. 68, 76–84.
Jault, D., Gire, C., Le Mouël, J.L., 1988. Westward drift, core motions and exchanges of angular momentum between core and mantle. Nature 333, 353–356.
King, E.M., Buffett, B.A., 2013. Flow speeds and length scales in geodynamo models: the role of viscosity. Earth Planet. Sci. Lett. 371–372, 156–162. http://dx.doi.org/10.1016/j.epsl.2013.04.001.
Larmor, J., 1919. How could a rotating body such as the sun become a magnet? Rep. Br. Assoc. Adv. Sci., 159–160
Le Huy, M., Alexandrescu, M., Hulot, G., Le Mouël, J.L., 1998. On the characteristics of successive geomagnetic jerks. Earth Planets Space 50, 723–732.
Le Mouël, J.L., 1984. Outer-core geostrophic flow and secular variation of Earth's geomagnetic field. Nature 311, 734–735.
Lesur, V., Whaler, K., Wardinski, I., 2015. Are geomagnetic data consistent with stably stratified flow at the core–mantle boundary? Geophys. J. Int. 201, 929–946. http://dx.doi.org/10.1093/gji/ggv031.
Lewis, H.R., Bellan, P.M., 1990. Physical constraints on the coefficients of Fourier expansions in cylindrical coordinates. J. Math. Phys. 31, 2592–2596.
Livermore, P.W., Hollerbach, R., 2012. Successive elimination of shear layers by a hierarchy of constraints in inviscid spherical-shell flows. J. Math. Phys. 53, 073104.
Macmillan, S., 1996. A geomagnetic jerk for the early 1990s. Earth Planet. Sci. Lett. 137, 189–192.
Malin, S.R.C., Hodder, B.M., 1982. Was the 1970 geomagnetic jerk of internal or external origin? Nature 296, 726–728.
Malin, S.R.C., Hodder, B.M., Barraclough, D.R., 1983. Geomagnetic secular variation: a jerk in 1970. In: Scientific Contributions in Commemoration of Ebro Observatory's 75th Anniversary. pp. 239–256.
Malkin, Z., 2013. Free core nutation and geomagnetic jerks. J. Geodyn. 72, 53–58.
Mandea, M., Bellanger, E., Le Mouël, J.L., 2000. A geomagnetic jerk for the end of the 20th century? Earth Planet. Sci. Lett. 183, 369–373.
Mandea, M., Holme, R., Pais, A., Pinheiro, K., Jackson, A., Verbanac, G., 2010. Geomagnetic jerks: rapid core field variations and core dynamics. Space Sci. Rev. 155, 147–175.
Matzka, J., Chulliat, A., Mandea, M., Finlay, C., Qamili, E., 2010. Geomagnetic observations for main field studies: from ground to space. Space Sci. Rev. 155, 29–64.
Mound, J.E., Buffett, B.A., 2005. Mechanisms of core–mantle angular momentum exchange and the observed spectral properties of torsional oscillations. J. Geophys. Res.: Solid Earth 1978–2012, 110.
Mound, J., Buffett, B., 2007. Viscosity of the Earth's fluid core and torsional oscillations. J. Geophys. Res. 112, B05402.
Olsen, N., Mandea, M., 2007. Investigation of a secular variation impulse using satellite data: the 2003 geomagnetic jerk. Earth Planet. Sci. Lett. 255, 94–105.
Olsen, N., Mandea, M., 2008. Rapidly changing flows in the Earth's core. Nat. Geosci. 1, 390–394.
Olsen, N., Lühr, H., Finlay, C.C., Sabaka, T.J., Michaelis, I., Rauberg, J., Tffner-Clausen, L., 2014. The CHAOS-4 geomagnetic field model. Geophys. J. Int. 197, 815–827.
Pinheiro, K., Jackson, A., 2008. Can a 1-D mantle electrical conductivity model generate magnetic jerk differential time delays? Geophys. J. Int. 173, 781–792.
Pinheiro, K., Jackson, A., Finlay, C., 2011. Measurements and uncertainties of the occurrence time of the 1969, 1978, 1991, and 1999 geomagnetic jerks. Geochem. Geophys. Geosyst. 12.
Reda, J., Fouassier, D., Isac, A., Linthe, H.J., Matzka, J., Turbitt, C., 2011. Improvements in geomagnetic observatory data quality. In: Geomagnetic Observations and Models. In: Mandea, M., Korte, M. (Eds.), . IAGA Special Sopron Book Series, vol. 5. Springer, Netherlands, pp. 127–148. http://dx.doi.org/10.1007/978-90-481-9858-06.
Roberts, P.H., Aurnou, J.M., 2011. On the theory of core–mantle coupling. Geophys. Astrophys. Fluid Dyn. 106, 157–230.
Roberts, P., Scott, S., 1965. On analysis of the secular variation. A hydromagnetic constraint: theory. J. Geomagn. Geolect. 17, 137–151.
Roberts, P., Yu, Z., Russell, C., 2007. On the 60 year signal from the core. Geophys. Astrophys. Fluid Dyn. 101, 11–35.
Schaeffer, N., Jault, D., Cardin, P., Drouard, M., 2012. On the reflection of Alfvèn waves and its implication for Earth's core modelling. Geophys. J. Int. 191, 508–516. http://dx.doi.org/10.1111/j.1365-246X.2012.05611.x.
Shankland, T.J., Peyronneau, J., Poirer, J.P., 1993. Electrical conductivity of the Earth's lower mantle. Nature 366, 453–455.
Shirai, T., Fukushima, T., Malkin, Z., 2005. Detection of phase disturbances of free core nutation of the Earth and their concurrence with geomagnetic jerks. Earth Planets Space 57, 151–155.
Silva, L., Hulot, G., 2012. Investigating the 2003 geomagnetic jerk by simultaneous inversion of the secular variation and acceleration for both the core flow and its acceleration. Phys. Earth Planet. Inter. 198, 28–50.
Teed, R.J., Jones, C.A., Tobias, S.M., 2013. The dynamics and excitation of torsional waves in geodynamo simulations. Geophys. J. Int. http://dx.doi.org/10.1093/gji/ggt432.
Teed, R.J., Jones, C.A., Tobias, S.M., 2015. The transition to Earth-like torsional oscillations in magnetoconvection simulations. Earth Planet. Sci. Lett. 419, 22–31. http://dx.doi.org/10.1016/j.epsl.2015.02.045.
Waddington, R., Gubbins, D., Barber, N., 1995. Geomagnetic field analysis V. Determining steady core-surface flows directly from geomagnetic observations. Geophys. J. Int. 122, 326–350.
Wardinski, I., Holme, R., 2011. Signal from noise in geomagnetic field modelling: denoising data for secular variation studies. Geophys. J. Int. 185, 653–662.
Wardinski, I., Holme, R., Asari, S., Mandea, M., 2008. The 2003 geomagnetic jerk and its relation to the core surface flows. Earth Planet. Sci. Lett. 267, 468–481.
Whaler, K., 1980. Does the whole of the Earth's core convect? Nature 287, 528–530.
Whaler, K.A., 1987. A new method for analysing geomagnetic impulses. Phys. Earth Planet. Int. 48, 221–240.
Whaler, K.A., Holme, R., 2007. Consistency between the flow at the top of the core and the frozen-flux approximation. Earth Planets Space 59, 1219–1229.
Wicht, J., Christensen, U.R., 2010. Torsional oscillations in dynamo simulations. Geophys. J. Int. 181, 1367–1380.
Zatman, S., Bloxham, J., 1997. Torsional oscillations and the magnetic field within the Earth's core. Nature 388, 760–763.
Zatman, S., Bloxham, J., 1999. On the dynamical implications of models of b_s in the Earth's core. Geophys. J. Int. 138, 679–686.